

Pole Analysis of the Inter-Replica Correlation Function in a Two-Replica System as a Binary Mixture: Mean Overlap in the Cluster Glass Phase

Hiroshi Frusawa*

Laboratory of Statistical Physics, Kochi University of Technology, Tosa-Yamada, Kochi 782-8502, Japan.

(Dated: July 16, 2024)

To investigate the cluster glass phase of ultrasoft particles, we examine an annealed two-replica system endowed with an attractive inter-replica field similar to that of a binary symmetric electrolyte. Leveraging this analogy, we conduct pole analysis on the total correlation functions in the two-replica system where the inter-replica field will eventually be switched off. By synthesizing discussions grounded in the pole analysis with a hierarchical view of the free-energy landscape, we derive an analytical form of the mean overlap between two replicas within the mean field approximation of the Gaussian core model. This formula elucidates novel numerical findings observed in the cluster glass phase.

I. INTRODUCTION

Ultrasoft particles that may overlap and deform offer a powerful model for understanding complex systems such as polymers, dendrimers, and two-dimensional bosons [1–5]. The theoretical and simulation results on the soft-core models have revealed new and surprising features, including clustering phenomena and reentrant phase behaviors [1–23]. For example, the generalized exponential model (GEM) adopts an ultrasoft potential $v(r)$ in units of $k_B T$ as follows:

$$v(r) = \tilde{\epsilon} \exp\{-r^s\}, \quad (1)$$

where interparticle distance r is measured in units of a characteristic length d , $\tilde{\epsilon}$ corresponds to a dimensionless interaction strength at zero separation, and the potential profile is characterized by a softness exponent s [6–23].

Especially for $s > 2$ of the GEM, or the so-called Q^\pm class, the non-positive definiteness of the Fourier transform $v(k)$ of $v(r)$ leads to the formation of equilibrium clusters in the liquid, crystalline, and glass phases, as confirmed by theoretical and simulation studies [6–23]. Meanwhile, the complementary class (Q^+ class) of the GEM for $s \leq 2$ does not form clusters in equilibrium due to the positive definite Fourier transform (i.e., $v(k) > 0$) [6–23]. Recently, however, the glass phase of the GEM at $s = 2$, or the Gaussian core model (GCM), has been investigated using two copies of replicated systems (two-replica system), thereby demonstrating the occurrence of local aggregates or out-of-equilibrium clusters in the glass phase [22, 23].

We are concerned with the cluster-forming glassy states of soft-core models, particularly the GEM of ultrasoft particles interacting via $v(r)$ irrespective of whether $v(r)$ given by Equation (1) belongs to the Q^\pm class ($s > 2$) or the Q^+ class ($s \leq 2$).

The cluster-forming states tend to emerge at higher densities where the supercooled ultrasoft systems behave as mean-field fluids [6–23]. Correspondingly, experimental and simulation studies on single-particle dynamics in the cluster glasses have revealed the following hierarchical feature, other than the cage-hopping dynamic characteristic of non-cluster-forming supercooled liquids: while the cooperative dynamics are ascribed to the freezing of clusters' center of mass, the single-particle dynamics include inter-cluster hopping and intra-cluster fluctuations [23–28]. The blurring of cage-hopping dynamics in the high-density region is similar to that of the short-time dynamics in the marginal glass phase [29–35]. While a stable glass has a plateau in the mean squared displacement (MSD) that decreases with increasing density, a marginal glass exhibits a logarithmic growth of the MSD with lag time [29–35]. The former represents the crossover from ballistic motion to caged behavior, whereas the latter indicates that particles leave small cages to find themselves in slightly larger cages: cages themselves are ever-shifting [29–35].

For comparison, it is helpful to see the stable and marginal glasses in terms of the free-energy landscape (FEL) [29–35]. On the one hand, the FEL in the stable glass state consists of many smooth basins separated by energy barriers. The single-particle dynamics in the stable glass include rattling inside an arrested cage and cage-to-cage hopping, which are interpreted as vibrational excitations around each basin and jumps between different basins, respectively. The marginal glass, on the other hand, provides infinitesimally different metastable states, reflecting the

*Electronic address: frusawa.hiroshi@kochi-tech.ac.jp

hierarchical FEL where the basin splits into a fractal hierarchy of sub-basins [29–35]. As a result, even an infinitesimal perturbation can trigger a transition between adjacent similar metastable states. The above dynamical similarity between the cluster-forming and marginal glasses suggests that it is relevant to consider the hierarchical FEL [29–35] when addressing the two-scale fluctuations in cluster-forming glasses.

Here, we develop a theoretical framework for the two-replica system without a quenched disorder, or the annealed two-replica system [36–49], in the cluster-forming glassy states. Our focus is on the pole analysis [50–55] of density–density correlation functions considering the hierarchical FEL. The previous results demonstrate the usefulness of the pole analysis when investigating fluctuations separately by length scales. For example, the pole analysis method applies to a fluid mixture with competing interactions that cause cluster formation, thereby detecting the change in density–density correlation functions from monotonic to damped oscillatory decay [50–62]; the fluid mixture undergoes continuous transitions to a state characterized by periodic concentration fluctuations (microphase separation). A combined approach of the pole analysis and FEL would thus be relevant to investigate the annealed two-replica system [43–49] in the cluster-forming glassy states where the cage-to-cage hopping is obscured [23–28].

This paper is organized as follows. In Section II, we introduce mean overlap as an index by which to measure similarity between two replicas and express it using total correlation functions (TCFs). In Section III, we conduct the pole analysis of TCFs, providing novel results that generally apply to two-replica systems in glassy states. Section IV demonstrates that the pole-analysis-based discussions allow us to determine the TCFs without solving the Ornstein–Zernike (OZ) equations. In Section V, we consider the FEL in the cluster glass phase for revealing the underlying physics of TCFs obtained from the pole-analysis-based discussions. In Section VI, we assess the validity of the pole-analysis-based results, focusing on the GCM in the mean field approximation. Section VII makes some concluding remarks.

II. TWO-REPLICA SYSTEM: BASIC FORMULATION

This section introduces mean overlap and TCF, characteristic quantities of the two-replica system [36–49]. First, in Section II A, we define the mean overlap using a density correlation function as an index by which to measure the similarity between two replicas. Next, in Section II B, based on the analogy with symmetric binary electrolytes, two replicas are characterized by the average density, the difference density (corresponding to the charge density in electrolytes), and the associated TCFs that provide intra- and inter-replica ones. Finally, in Section II C, we present the OZ equations for symmetric binary mixtures [45–49, 55], which allows us to express TCFs of average and difference densities using the direct correlation functions (DCFs).

A. Mean Overlap

Let $\hat{\rho}_\alpha(\mathbf{x}) = \sum_{i=1}^N \delta[\mathbf{x} - \mathbf{r}_\alpha^i]$ be a microscopic density in replica $\alpha \in \{1, 2, \dots, n\}$ of the N -particle system with the volume V when considering the i th-particle located at \mathbf{r}_α^i ($1 \leq i \leq N$). The mean overlap $Q_{\alpha\beta}$ represents the degree of similarity between configurations of replica α and replica β . We define $Q_{\alpha\beta}$ as

$$Q_{\alpha\beta} = \frac{d^6}{N} \iint d\mathbf{x} d\mathbf{y} \Theta(l - r) \langle \hat{G}_{\alpha\beta}(r) \rangle, \quad (2)$$

$$\hat{G}_{\alpha\beta}(r) = \hat{\rho}_\alpha(\mathbf{x}) \hat{\rho}_\beta(\mathbf{y}) \quad (\alpha \neq \beta), \quad (3)$$

where $r \equiv |\mathbf{x} - \mathbf{y}|$, the Heaviside function $\Theta(l - r)$ is used to exclude the region of $r > l$, and the brackets denote the statistical average over the realizations of particle configurations [36–49].

While the replica trick for structural glasses eventually takes the limit of either $n \rightarrow 0$ or $n \rightarrow 1$ for the number of replicas [42], this paper is concerned with the mean overlap at $n = 2$. The two-replica overlap can also be an indicator of glassy states by switching on and off the inter-replica attractive field, similar to the role of a magnetic field in studying magnetization. Introducing an external field $-\tilde{\epsilon}_{12}$ conjugate to the mean overlap, Equation (2) allows us to write the inter-replica attractive energy U_{att} in units of $k_B T$ as

$$U_{\text{att}} = -N\tilde{\epsilon}_{12}Q_{12} \quad (4)$$

for the two-replica system. The attractive inter-replica field $-\tilde{\epsilon}_{12}$ plays different roles in the quenched and annealed systems. While the quenched system in replica 1 is studied in the presence of a quenched disorder created by a reference configuration of replica 2 drawn from the equilibrium distribution [36–42], the annealed system considers configurations of two replicas fluctuating simultaneously [43–49]: $-\tilde{\epsilon}_{12}$ acts on one of the replicas and both replicas in the quenched and annealed dynamics, respectively.

In the annealed system [43–49], the two-replica system can simply be regarded as a binary symmetric electrolyte [55]. This analogy allows us to predict that complexation between particles in replicas 1 and 2 occurs at sufficiently low temperatures due to the inter-replica attraction energy $-N\tilde{\epsilon}_{12}Q_{12}$. It has also been demonstrated that such complexes remain stable in the glass phase even when $\tilde{\epsilon}_{12}$ is progressively lowered from the initial value to zero (i.e., $\tilde{\epsilon}_{12} \rightarrow 0$), providing a non-trivial value of Q_{12} that is larger than the random overlap Q_r evaluated at $\langle \hat{G}_{\alpha\beta}(r) \rangle = \bar{\rho}^2$ using the uniform density $\bar{\rho} = N/V$. It follows from Equation (2) that

$$Q_r = \frac{4\pi}{3}\phi(ld)^3, \quad (5)$$

$$\phi = \bar{\rho}d^3, \quad (6)$$

where ϕ denotes the volume fraction [6–23, 43–49].

B. Two Replicas as a Binary Mixture: Density–Density Correlations

In the annealed two-replica system, it is natural to introduce another set of coarse-grained density variables related to the sum and difference, similar to a symmetric electrolyte [55]:

$$\hat{\rho}_+(\mathbf{r}) = \frac{1}{2}\{\hat{\rho}_1(\mathbf{r}) + \hat{\rho}_2(\mathbf{r})\}, \quad (7)$$

$$\hat{\rho}_-(\mathbf{r}) = \frac{1}{2}\{\hat{\rho}_1(\mathbf{r}) - \hat{\rho}_2(\mathbf{r})\}, \quad (8)$$

which will be called p -density and n -density, respectively, after the subscripts of positive and negative signs. As seen from the above definitions, the mean p -density $\langle \hat{\rho}_+(\mathbf{r}) \rangle$ corresponds to the average density of two replicas, whereas the mean n -density $\langle \hat{\rho}_-(\mathbf{r}) \rangle$ is a measure of local charge density in analogy with symmetric electrolytes. Accordingly, the uniform distribution results in $\langle \hat{\rho}_+(\mathbf{r}) \rangle = \bar{\rho}$ and $\langle \hat{\rho}_-(\mathbf{r}) \rangle = 0$.

We investigate the binary cluster glasses in the limit of $\tilde{\epsilon}_{12} \rightarrow 0$ using the p - p and n - n TCFs. Given that

$$\langle \hat{G}_{\alpha\beta}(r) \rangle = \bar{\rho}^2 \{1 + h_{\alpha\beta}(r)\} \quad (9)$$

for the TCF $h_{\alpha\beta}(r)$ between replica α and replica β , we have

$$\langle \hat{G}_{++}(r) \rangle = \bar{\rho}^2 \{1 + h_+(r)\}, \quad (10)$$

$$\langle \hat{G}_{--}(r) \rangle = \bar{\rho}^2 h_-(r), \quad (11)$$

respectively, where

$$\hat{G}_{++}(r) = \frac{1}{4} \{ \hat{G}_{11}(r) + 2\hat{G}_{12}(r) + \hat{G}_{22}(r) \}, \quad (12)$$

$$\hat{G}_{--}(r) = \frac{1}{4} \{ \hat{G}_{11}(r) - 2\hat{G}_{12}(r) + \hat{G}_{22}(r) \}, \quad (13)$$

due to Equations (7) and (8), and the TCFs $h_+(r)$ and $h_-(r)$ are defined by Equations (10) and (11).

The symmetric system also allows us to introduce the intra- and inter-replica TCFs, $h(r)$ and $\tilde{h}(r)$, given by

$$h(r) = h_{11}(r) = h_{22}(r), \quad (14)$$

$$\tilde{h}(r) = h_{12}(r) = h_{21}(r), \quad (15)$$

respectively.

It follows from Equations (9)–(15) that

$$h(r) = h_+(r) + h_-(r), \quad (16)$$

$$\tilde{h}(r) = h_+(r) - h_-(r). \quad (17)$$

Equation (17) implies that the inter-replica TCF $\tilde{h}(r)$ has a non-zero value when there is a difference between the p - p and n - n correlations even without inter-replica attractive interactions (i.e., $\tilde{\epsilon}_{12} = 0$). Plugging Equations (9) and (15) into Equation (2), we have

$$Q_{12} = Q_r + 4\pi\phi \int_0^l dr r^2 \tilde{h}(r). \quad (18)$$

The main purpose of this paper is to calculate the mean overlap Q_{12} using the inter-replica TCF $\tilde{h}(r)$ in Equation (18).

C. The Ornstein–Zernike Equations in Symmetric Binary Mixtures

The OZ equations in Fourier space relate the TCFs to the intra- and inter-replica DCFs denoted by $c(k)$ and $\tilde{c}(k)$, respectively, as follows [45–49]:

$$h(k) = c(k) + \bar{\rho} \left\{ c(k)h(k) + \tilde{c}(k)\tilde{h}(k) \right\}, \quad (19)$$

$$\tilde{h}(k) = \tilde{c}(k) + \bar{\rho} \left\{ c(k)\tilde{h}(k) + \tilde{c}(k)h(k) \right\}, \quad (20)$$

which apply to the two-replica system at $n = 2$. Meanwhile, Equations (16) and (17) read

$$h_+(k) = \frac{1}{2} \left\{ h(k) + \tilde{h}(k) \right\}, \quad (21)$$

$$h_-(k) = \frac{1}{2} \left\{ h(k) - \tilde{h}(k) \right\}. \quad (22)$$

Substituting Equations (19) and (20) into the right-hand sides (RHSs) of Equations (21) and (22), we have

$$h_+(k) = \frac{1}{2} \left\{ \frac{c_+(k)}{1 - \bar{\rho}c_+(k)} \right\}, \quad (23)$$

$$h_-(k) = \frac{1}{2} \left\{ \frac{c_-(k)}{1 - \bar{\rho}c_-(k)} \right\}, \quad (24)$$

when defining that

$$c_+(k) = c(k) + \tilde{c}(k), \quad (25)$$

$$c_-(k) = c(k) - \tilde{c}(k). \quad (26)$$

We will conduct the pole analysis of Equations (23) and (24).

III. POLE ANALYSIS: GENERAL RESULTS

Conducting the pole analysis [50–55] of Equations (23) and (24), we can find novel results that generally apply to two-replica systems in glassy states. In Section III A, we obtain the pole equations for glassy states, revealing new findings of density fluctuations. In Section III B, we present requirements for the inter-replica TCF in real and Fourier spaces, based on physical considerations.

A. Pole Equations

Considering that the real-space representation $c_\sigma(r)$ ($\sigma = +$ or $-$) of the DCF decays faster than a power law for finite-ranged or exponentially decaying interaction potentials, the TCF given by either Equation (23) or Equation (24) have poles at complex wavenumbers, $k_m^\sigma = a_m^\sigma + ib_m^\sigma$ ($m = 1, 2, \dots$) [50–55]. The integrated representation of pole equations is

$$\begin{aligned} 1 - \bar{\rho}c_\sigma(k_m^\sigma) &= 1 - \bar{\rho} \left\{ c(k_m^\sigma) + \sigma\tilde{c}(k_m^\sigma) \right\} \\ &= 0, \end{aligned} \quad (27)$$

providing the m th pole of $h_\sigma(k)$ given by either Equation (23) for $\sigma = +$ or Equation (24) for $\sigma = -$.

It follows from the OZ Equation (20) that the inter-replica DCF reads

$$\bar{\rho}\tilde{c}(k) = \{1 - \bar{\rho}c(k)\} \frac{\bar{\rho}\tilde{h}(k)}{1 + \bar{\rho}h(k)}. \quad (28)$$

Plugging Equation (28) into the RHS of the first line in Equation (27), the m th pole equation becomes

$$\begin{aligned} & \{1 - \bar{\rho}c(k_m^\sigma)\} \left\{ 1 - \frac{\sigma\bar{\rho}\tilde{h}(k_m^\sigma)}{1 + \bar{\rho}h(k_m^\sigma)} \right\} \\ &= \frac{1 - \bar{\rho}c(k_m^\sigma)}{1 + \bar{\rho}h(k_m^\sigma)} \left[1 + \bar{\rho} \left\{ h(k_m^\sigma) - \sigma\tilde{h}(k_m^\sigma) \right\} \right] \\ &= 0. \end{aligned} \quad (29)$$

In the supercooled liquid state, Equation (29) reduces to

$$1 - \bar{\rho}c(k_m) = 0, \quad (30)$$

because of $\tilde{h}(k) = 0$; we find from the Fourier transform of Equation (17) that $k_m = k_m^+ = k_m^-$ is a sufficient condition for $\tilde{h}(k) = 0$.

Meanwhile, in a glassy state where $\tilde{h}(k) \neq 0$, Equation (29) provides another equation,

$$1 + \bar{\rho} \left\{ h(k_m^\sigma) - \sigma\tilde{h}(k_m^\sigma) \right\} = 0, \quad (31)$$

in addition to Equation (30), or

$$\tilde{c}(k_m) = 0 \quad (32)$$

due to the original pole Equation (27). Equations (23)–(32) indicate the following:

- Combining Equations (23), (24), (27), and (31), it becomes apparent that a sign reversal occurs in glassy states: the pole equation for $c_\sigma(k)$ becomes that for $h_{-\sigma}(k)$.
- Equations (30)–(32) imply that there are two kinds of poles for TCFs, $h_+(k)$ and $h_-(k)$, in glassy states: one type is constituted by some of the same poles as those in the liquid state, and the other by the poles satisfying Equation (31).

It is instructive to examine the underlying physics of the pole equation expressed by Equation (31). To do so, we introduce the structure factors as follows:

$$S(k) = N^{-1} \langle \hat{\rho}_\alpha(k) \hat{\rho}_\alpha(-k) \rangle, \quad (33)$$

$$\tilde{S}(k) = N^{-1} \langle \hat{\rho}_\alpha(k) \hat{\rho}_\beta(-k) \rangle \quad (\alpha \neq \beta), \quad (34)$$

$$S_\sigma(k) = N^{-1} \langle \hat{\rho}_\sigma(k) \hat{\rho}_\sigma(-k) \rangle, \quad (35)$$

for $1 \leq \alpha, \beta \leq 2$, and $\sigma = +$ or $-$. Considering the density relations in Equations (7) and (8), Equations (33)–(35) yield

$$S_\sigma(k) = \frac{1}{2} \left\{ S(k) + \sigma\tilde{S}(k) \right\}, \quad (36)$$

which becomes

$$\begin{aligned} S_\sigma(k) &= \frac{1}{2} \left\{ 1 + \bar{\rho}h(k) + \sigma\bar{\rho}\tilde{h}(k) \right\} \\ &= \frac{1}{2} + \bar{\rho}h_\sigma(k), \end{aligned} \quad (37)$$

noting that $S(k) = 1 + \bar{\rho}h(k)$ and $\tilde{S}(k) = \bar{\rho}\tilde{h}(k)$ as well as the definition of $h_\sigma(k)$ in Equation (21) or Equation (22). Combining Equations (31) and (37), we have

$$S_-(k_m^+) = 0, \quad (38)$$

$$S_+(k_m^-) = 0. \quad (39)$$

Sign reversals appear in Equations (38) and (39), as mentioned above: $S_\sigma(k)$ as a function of complex wave number k equals zero at a complex wavenumber of $k_m^{-\sigma}$.

Among our main theoretical findings are Equations (38) and (39). The mixed relationship implies the following characteristics of glassy states:

- *Opposite phenomena: the enhancement of p -density fluctuations at k_m^+ leads to the suppression of n -density fluctuations and vice versa, which creates the inter-replica correlations.*
- *Exclusive poles: the above reverse trend in density fluctuations indicates that there are unique poles k_m^σ that $h_+(k)$ and $h_-(k)$ do not share with each other.*

Section V C will relate the exclusive poles to characteristic lengths of cluster glasses.

B. Two Requirements

The poles determined by Equations (38) and (39) allow us to perform the 3D Fourier transform of Equations (23) and (24) using contour integral along an infinite radius semicircle in the complex upper half-plane. Remembering that $k_m^\sigma = a_m^\sigma + ib_m^\sigma$ ($m = 1, 2, \dots$) at poles, the pole analysis provides [50–52]

$$rh_\sigma(r) = \sum_{m \geq 1} A_m^\sigma e^{-b_m^\sigma r} \cos(a_m^\sigma r + \theta_m^\sigma), \quad (40)$$

indicating that $(b_m^\sigma)^{-1}$ corresponds to the decay length. We use the pole series in order of decreasing decay lengths: $b_m^\sigma < b_{m+1}^\sigma$. The contribution from the m th pole in Equation (40) will be referred to as the m th mode.

Let $h_\sigma^{\text{liq}}(r)$ and $h^{\text{liq}}(r)$ denote TCFs of the supercooled liquid before vitrification. Equation (17) implies that there is no difference between $h_+^{\text{liq}}(r)$ and $h_-^{\text{liq}}(r)$ because of the absence of the inter-replica TCF in the supercooled liquid state. Therefore, Equation (40) reduces to

$$rh_+^{\text{liq}}(r) = rh_-^{\text{liq}}(r) = \sum_{m \geq 1} A_m e^{-b_m r} \cos(a_m r + \theta_m), \quad (41)$$

for $k_m = a_m + ib_m$, satisfying Equation (30). Combining Equations (16) and (41), the intra-replica TCF $h^{\text{liq}}(r)$ in the supercooled liquid state becomes

$$rh^{\text{liq}}(r) = \sum_{m \geq 1} 2A_m e^{-b_m r} \cos(a_m r + \theta_m), \quad (42)$$

where the m th mode is determined by the pole Equation (30).

It has been confirmed that the above type of expansion form based on the pole analysis correctly yields the correlation functions in the liquid state [50–55]. It has also been found that liquids and glasses are indistinguishable from each other in terms of two-body density correlation: there is little structural change accompanying the slowdown of the dynamics of supercooled liquids.

The above structural feature leads to the requirement [RR] on glassy states in real space:

$$[\text{RR}] \quad h(r) = h_+(r) + h_-(r) = h^{\text{liq}}(r),$$

similar to $h_+^{\text{liq}}(r) + h_-^{\text{liq}}(r) = h^{\text{liq}}(r)$ in Equation (42), while producing

$$\tilde{h}(r) = h_+(r) - h_-(r) \neq 0 \quad (43)$$

by definition of glassy states. The real-space requirement [RR] with Equations (42) and (43) states that the sum of $h_+(r)$ and $h_-(r)$ in glassy states is constituted by the liquid-state modes represented by k_m , despite making a difference between $h_+(r)$ and $h_-(r)$.

In Fourier space, on the other hand, Equations (30) and (31), as well as the real-space requirement [RR], imply that the glassy poles given by Equation (31) must satisfy Equations (30) and (32) simultaneously; otherwise, the exclusive modes other than the liquid-state ones necessarily remain by adding $h_+(r)$ and $h_-(r)$ against the real-space requirement [RR] because of the exclusive poles explained at the end of Section III A. The constraint [RR] therefore applies only to solutions that satisfy Equations (30) to (32) simultaneously. Thus, the Fourier space requirement [FR],

or another expression of the real-space one [RR], is that the pole Equations (38) and (39) for glassy states must hold at a subset of k_m satisfying Equation (30), or liquid-state modes:

$$[\text{FR}] \quad S_-(k_\nu) = 0, \quad S_+(k_{\nu'}) = 0,$$

for $\nu, \nu' \subset m$ with $\nu \neq \nu'$. It is to be remembered from Equations (38) and (39) that k_ν corresponds to the pole of $h_+(k)$ and $k_{\nu'}$ to that of $h_-(k)$.

IV. INTER-REPLICA TOTAL CORRELATION FUNCTION

This section demonstrates that the pole-analysis-based discussions allow us to determine the inter-replica TCF $\tilde{h}(r)$ without finding out-of-equilibrium solutions to the OZ Equations (19) and (20). In Section IV A, we obtain a general form of the inter-replica TCF in real space by combining the requirements [RR] and [FR]. Furthermore, we confirm that the pole Equations (30) to (32) yield the Fourier transform of the general expression. In Section IV B, we propose a two-mode model considering the two-scale dynamics in cluster glasses.

A. General Form

The two requirements, [RR] and [FR], provide

$$r\tilde{h}(r) = \sum_{\nu} 2A_{\nu}e^{-b_{\nu}r} \cos(a_{\nu}r + \theta_{\nu}) - \sum_{\nu'} 2A_{\nu'}e^{-b_{\nu'}r} \cos(a_{\nu'}r + \theta_{\nu'}). \quad (44)$$

Equations (42) and (44) satisfy Equations (16) and (17) by taking the following forms:

$$rh_+(r) = \sum_m A_m e^{-b_m r} \cos(a_m r + \theta_m) + \frac{r\tilde{h}(r)}{2}, \quad (45)$$

$$rh_-(r) = \sum_m A_m e^{-b_m r} \cos(a_m r + \theta_m) - \frac{r\tilde{h}(r)}{2}. \quad (46)$$

Equation (44) corresponds to a general expression of the inter-replica TCF $\tilde{h}(r)$ obtained from the pole-analysis-based discussions. It is noted that the ν' th mode disappears in Equation (45) and the ν th mode in Equation (46); therefore, the expressions (45) and (46) ensure the validity of not only the real-space requirement [RR] but also the Fourier space one [FR].

The general form (44) implies that

$$\lim_{k \rightarrow k_{\nu}} \tilde{h}(k) = \lim_{k \rightarrow k_{\nu}} h_+(k) = \infty, \quad (47)$$

$$\lim_{k \rightarrow k_{\nu'}} \tilde{h}(k) = - \lim_{k \rightarrow k_{\nu'}} h_-(k) = -\infty, \quad (48)$$

where it is noted that the wavenumbers, k_{ν} and $k_{\nu'}$, are a subset of k_m that represents solutions to Equation (30) (i.e., $\nu, \nu' \subset m$). We show below that the limiting behaviors of Equations (47) and (48) can be derived from the pole Equations (30)–(32) that are satisfied simultaneously at k_{ν} and $k_{\nu'}$ in accordance with the requirement [FR].

The pole Equation (31), or the requirement [FR], reads

$$\bar{\rho}\tilde{h}(k_{\nu}) = 1 + \bar{\rho}h(k_{\nu}), \quad (49)$$

$$-\bar{\rho}\tilde{h}(k_{\nu'}) = 1 + \bar{\rho}h(k_{\nu'}). \quad (50)$$

Plugging either Equation (49) or Equation (50) into Equation (19), we obtain

$$h(k_{\nu}) = c(k_{\nu}) + \tilde{c}(k_{\nu}) + \bar{\rho} \{c(k_{\nu}) + \tilde{c}(k_{\nu})\} h(k_{\nu}), \quad (51)$$

$$h(k_{\nu'}) = c(k_{\nu'}) - \tilde{c}(k_{\nu'}) + \bar{\rho} \{c(k_{\nu'}) - \tilde{c}(k_{\nu'})\} h(k_{\nu'}). \quad (52)$$

It follows from Equations (49) to (52) that Equation (31) becomes

$$\tilde{\rho}h(k_\nu) = \frac{1}{1 - \tilde{\rho}c_+(k_\nu)}, \quad (53)$$

$$\tilde{\rho}h(k_{\nu'}) = -\frac{1}{1 - \tilde{\rho}c_-(k_{\nu'})}, \quad (54)$$

amounting to the limiting behaviors of Equations (47) and (48) because of Equations (30) and (32) valid at k_ν and $k_{\nu'}$. Remarkably, it has been proved that k_ν and $k_{\nu'}$ are the poles in the liquid state. Nevertheless, cancellation between $h_+(k)$ and $h_-(k)$ does not occur, and we can adjust the sum of $h_+(k)$ and $h_-(k)$ to yield $h^{\text{liq}}(k)$ (i.e., $h_+(k) + h_-(k) = h^{\text{liq}}(k)$), according to the requirement [RR].

Figure 1 puts together the discussions we have had so far about the two requirements, [RR] and [FR], as well as Equations (44) to (54). Figure 1 clarifies the whole discussion for the general formalism, which could help us understand the overall scheme providing Equation (44).

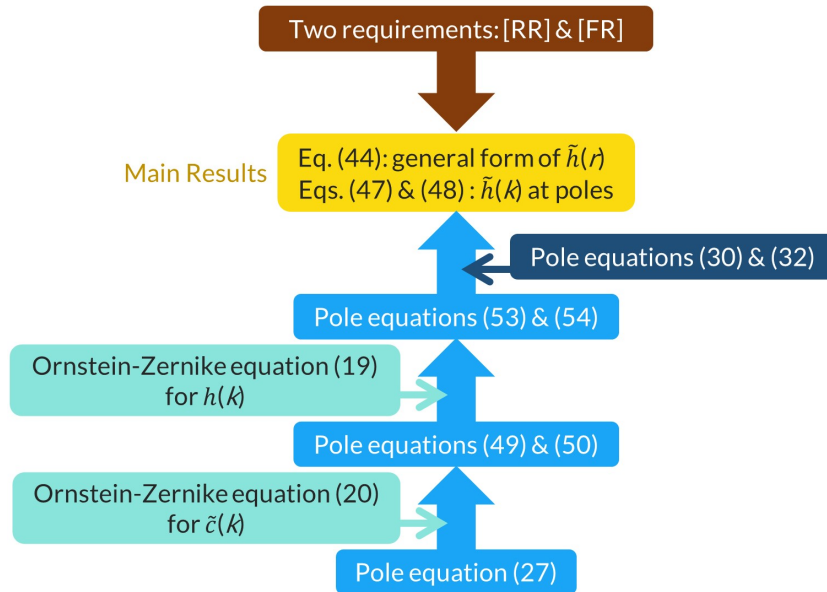


FIG. 1: A schematic summary of general formalism to obtain the main results represented by Equations (44) to (48).

B. Two-Mode Selection as a Minimal Model

As mentioned in Section I, previous studies have confirmed that cluster glasses are characterized by two scales: cluster and cage sizes. Focusing on these scales significant for the dynamical and structural properties, we can establish a minimal model reflecting this particularity: we select two modes of $\nu = \mu$ and $\nu' = \mu'$, thereby reducing Equation (44) to

$$r\tilde{h}(r) = 2A_\mu e^{-b_\mu r} \cos(a_\mu r + \theta_\mu) - 2A_{\mu'} e^{-b_{\mu'} r} \cos(a_{\mu'} r + \theta_{\mu'}). \quad (55)$$

Equation (55) implies that $b_\mu < b_{\mu'}$ is necessary for the first term on the rhs of Equation (55) to determine the overall behavior of $\tilde{h}(r)$. In other words, the decay length b_μ^{-1} for p - p density fluctuations must be longer than that $b_{\mu'}^{-1}$ for n - n density ones.

Equation (55) gives the inter-replica TCF at zero separation as follows:

$$\tilde{h}(0) = 2A(b_{\mu'} - b_\mu) + 2A(\delta - \delta') \lim_{r \rightarrow 0} \frac{1}{r}, \quad (56)$$

where

$$\begin{aligned} A_\mu \cos \theta_\mu &= A(1 + \delta), \\ A_{\mu'} \cos \theta_{\mu'} &= A(1 + \delta'), \end{aligned} \quad (57)$$

for $b_\mu < b_{\mu'}$. We see from (56) that $\tilde{h}(0) > 0$ for $\delta \geq \delta'$. The relation $\tilde{h}(0) > 0$ indicates that there are particles of different replicas that interpenetrate each other; $\tilde{h}(r)$ in Equation (55) adequately describes the cluster glass phase where clusters are formed by molecules of two replicas, hence reaching a value of mean overlap such that $Q_{12} \gg Q_r$.

Table I is another summary of our results on the two-mode model using the structure factors: $S_\sigma(k)$ ($\sigma = +, -$). Table I classifies the modes into three groups (the μ th, the μ' th, and the other modes) that have different characteristics in terms of density fluctuations at different wavenumbers. Focusing on the μ th mode in Table I, as well as the above inequality $b_\mu^{-1} > b_{\mu'}^{-1}$, we see the opposite behavior as follows: the density correlation with its oscillation period of $2\pi/a_\mu$ is enhanced and long-ranged in terms of p -density TCF $h_+(r)$, whereas the fluctuations in n -density are suppressed completely at the scale of $2\pi/a_\mu$ (i.e., $S_-(k_\mu) = 0$), according to the Fourier space requirement [FR].

TABLE I: The structure factors, $S_+(k)$, and $S_-(k)$ in the two-mode model. Three kinds of modes are characterized by different behaviors of density fluctuations at the wavenumbers of k_μ (the μ th mode), $k_{\mu'}$ (the μ' th mode), and $k_{m \neq \mu, \mu'}$ (the other modes).

		$S_+(k)$	
		Equation (30): Divergence	Equation (38): Vanishing
$S_-(k)$	Equation (30): divergence	$k_{m \neq \mu, \mu'}$	$k_{\mu'}$
	Equation (39): vanishing	k_μ	—

Given a linkage between the μ th mode and the cluster scale, the vanishing structure factor of n -density suggests the neutralization of charge within each cluster due to the complexation of two-replica clusters. Accordingly, we find the other μ' th mode related to cage size. Section V will delve deeper into the physics underpinning the μ th and μ' th modes to elucidate their relationship with cluster and cage sizes with the help of FEL.

V. INSIGHTS FROM THE FREE-ENERGY LANDSCAPE

Prior to assessing the validity of Equation (55), we reveal the underlying physics of the two-mode model in the cluster glass phase with the help of FEL. Figure 2 exhibits different behaviors of glassy and supercooled liquid states using the FEL. In Figure 2a, the FEL for normal stable glasses is considered, illustrating how a single smooth basin breaks into multiple basins. Meanwhile, the bi-axial FEL in Figure 2b demonstrates that each basin is segmented into sub-basins. These sub-basins represent possible configurations of cages with clusters frozen in a specific configuration (see Sections V A and V B). The bi-axial FEL in Figure 2b also gives insight into the roles of fluctuations in p - and n -densities, based on which we relate the requirement [FR] in Section III B to cluster and cage sizes: ξ_L and ξ_S (see Section V C).

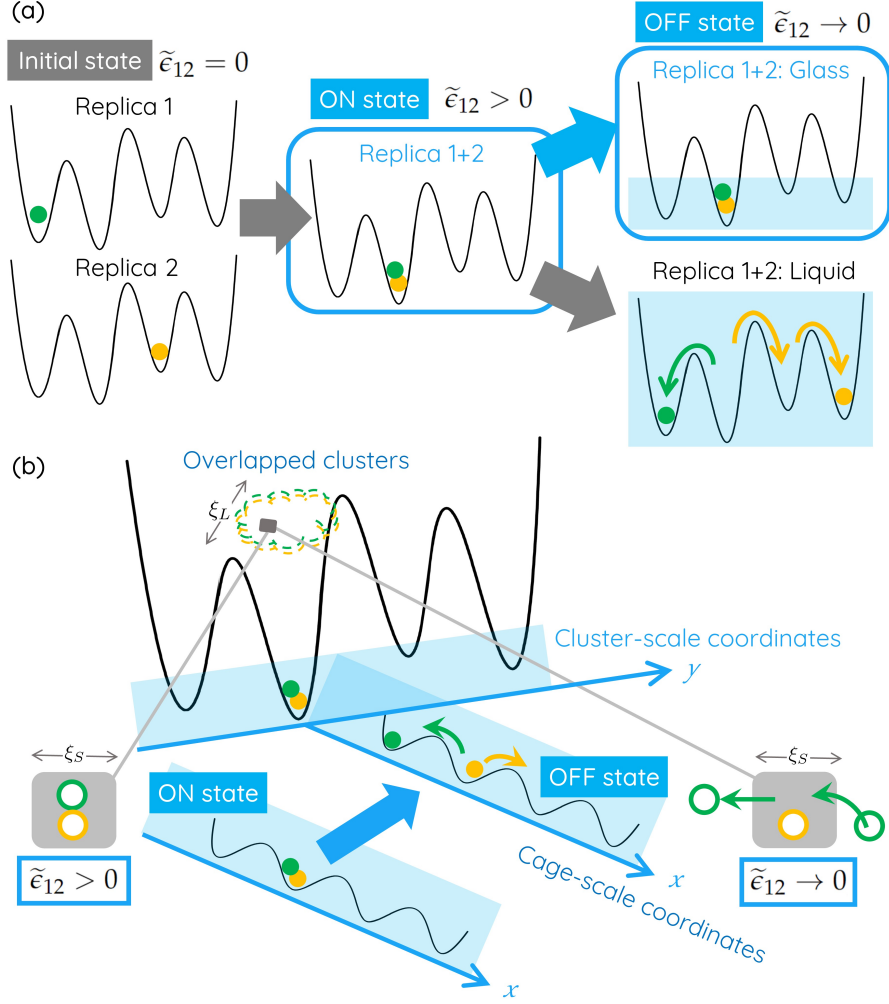


FIG. 2: Two-replica system in terms of the FEL. Green and orange circles in basins or sub-basins represent the states of different replicas. (a) There are three states (i.e., Initial and ON/OFF states) when considering a couple of replicated FELs (Initial state) and the merged FEL (ON/OFF states). Switching off the inter-replica attractive field ($\tilde{\epsilon}_{12} \rightarrow 0$), the ON state of two replicas in the same basin transforms to the OFF state, representing either a glass or supercooled liquid. On the one hand, two replicas trapped in the same basin represent a glass using shallow lakes separated by high mountains. On the other hand, two replicas in the liquid state can explore all configurational realizations independently because of the merging between the separated lakes. (b) The bi-axial FEL for a cluster-forming glassy state. The x - and y -axes denote particle coordinates on the scales of cage and cluster sizes (or ξ_s - and ξ_L -scales), respectively. The FEL in the x -axis direction has sub-basins shallower than water depth. In an OFF state, two replicas undergo independent transitions between the sub-basins while confined to the same basin.

A. The FEL for the Two-Replica System

Figure 2a shows the change of particle configurations in the replicated FELs of two replicas, which occurs in two steps associated with switching on and off the inter-replica attractive field. The first step is to apply the inter-replica attractive field (i.e., $-\tilde{\epsilon}_{12} < 0$) to the replicated FELs in an initial state at $\tilde{\epsilon}_{12} = 0$ of Figure 2a. As a consequence, we find two replicas in an identical state of the merged FEL (see an 'ON state' at $\tilde{\epsilon}_{12} > 0$ of Figure 2a). The second step is to switch off the inter-replica attractive field, creating an 'OFF state' at $\tilde{\epsilon}_{12} \rightarrow 0$ of Figure 2a.

The OFF state varies depending on whether the two replicas are initially in a glassy or supercooled liquid state. The supercooled liquid state allows for two replicas to jump from the initial basin to different ones independently, thereby amounting to non-overlapped configurations. Meanwhile, the glassy state maintains the ON state (the particle configurations in the ON state without the occurrence of transitions between adjacent basins) at $\tilde{\epsilon}_{12} \rightarrow 0$, which is suitable for describing the cage-hopping dynamics in normal stable glasses.

However, there is a difference in the particle dynamics of normal and cluster glass states. On the one hand, the dimer could maintain a molecular bound state in normal glasses where the cage-hopping dynamics are obviously observed; the particles of different replicas constituting the dimer are arrested in an overlapped cage even in the absence of the attractive inter-replica field (i.e., $\tilde{\epsilon}_{12} \rightarrow 0$). On the other hand, we have found the blurring of cage-hopping dynamics [23–28] in the cluster glass phase, indicating that the constituent particles of the dimer tend to be replaced by surrounding particles due to the loose cages. The FEL in the cluster glass phase should be modified to reflect the above difference.

B. Mixed State in Terms of the Bi-Axial FEL

In the marginal glass phase [29–35], previous theoretical studies have considered the hierarchical FEL where each basin in Figure 2a splits into sub-basins, thereby explaining the blurring of the cage-hopping dynamics as follows: transitions between adjacent sub-basins are triggered by switching off the inter-replica attractive field while frozen in the same basin. Considering the similarity between the particle dynamics in cluster and marginal glasses, we propose the bi-axial FEL in Figure 2b for adding shallow sub-basins for a cluster-forming state.

While the sub-basins along the x -axis represent a variety of cage configurations in a specific basin, the basins along the y -axis present various coarse-grained arrangements of clusters. Green and orange circles in the bi-axial FEL of Figure 2b denote glassy states of different replicas. These circles are located along the two axes, reflecting the hierarchical state of two-replica cluster glasses. It is helpful to compare Figure 2b and a set of two FELs in the rightmost column of Figure 2a, revealing a mixed state formed by clusters in a glassy state (y -axis) and constituent particles in a liquid state (x -axis).

Let us explain the mixed state in more detail. Focusing on the cluster scale ξ_L , overlapped clusters of two replicas would be indistinguishable from each other at ξ_L by definition of cluster glasses. The cluster complexation is represented by the FEL along the y -axis in Figure 2b: two replicas remain trapped at the same basin in the y -axis direction even after switching off the attractive interaction (i.e., $\tilde{\epsilon}_{12} \rightarrow 0$). Along the x -axis in Figure 2b, on the other hand, we depict sub-basins that are shallower than water depth, thereby illustrating the ON/OFF states that are distinguishable by whether transitions between sub-basins occur or not in the x -axis direction. Looking at the smaller scale of cage size ξ_S , a dimer formed by the inter-replica attractive field can be reconstituted in the OFF state of cluster glasses; that is, the single-particle dynamics induce dimer rearrangements inside the overlapped cluster at $\tilde{\epsilon}_{12} \rightarrow 0$ such that the blurring of the cage-hopping dynamics has been observed [23–28].

C. Characteristic Lengths in the Two-Mode Model

Let us consider the two-mode model in terms of the p - and n -density fluctuations, which vary according to the length scales (or the axes of the FEL in Figure 2b). The purpose here is to provide two characteristic lengths as candidates to create the two modes by revealing the underlying physics of the relations in [FR].

Two-replica systems exhibit two features when they belong to the same basin along the y -axis of Figure 2b. First, two replicas exhibit an identical inhomogeneity of the cluster-scale density distribution in contrast to the uniform liquid state where various configurations are possible. Second, the molecular bound state of replicated particles in a normal glass state is replaced by the complexation of replicated clusters in the cluster glass phase. The p -density, or the average density of two replicas, directly reflects the former feature. Meanwhile, regarding the latter characteristic, the cluster complexation of two replicas leads to the disappearance of n -density, or no net charge, per each overlapped cluster on average. Thus, ξ_L is related to the μ th mode, satisfying $S_-(k_\mu) = 0$ in [FR] as

$$a_\mu = \frac{2\pi}{\xi_L} \quad (58)$$

for the real part of the μ th wavenumber, $k_\mu = a_\mu + ib_\mu$, at which there is a pole of $h_+(k)$. Such uniformity and suppressed fluctuations in the n -density are in contrast to variations in cluster size and the number of particles forming each aggregate; the polydisperse clusters necessarily produce an inhomogeneous distribution of p -density, $\rho_+(\mathbf{r})$.

Turning our attention to the other length, the cage size ξ_S , we can see a dimer of different replicas. However, due to the cage-scale liquidity in the OFF state, replicas are located in different sub-basins along the x -axis, as illustrated in Figure 2b. Thus, we can suppose ξ_S to be a characteristic scale over which n -density fluctuations, including

spatiotemporal flip-flopping of charge sign, become apparent in the cluster glass phase:

$$a_{\mu'} = \frac{2\pi}{\xi_S} \quad (59)$$

for the real part of the μ' th wavenumber, $k_{\mu'} = a_{\mu'} + ib_{\mu'}$. Considering that the total particle number is fixed to be 2 per overlapped cage by definition, it is reasonable to satisfy $S_+(k_{\mu'}) = 0$ at $k_{\mu'} = a_{\mu'} + ib_{\mu'}$ while having a pole of $h_-(k)$ at $k_{\mu'}$.

VI. MEAN FIELD ANALYSIS OF THE GCM: ASSESSING THE TWO-MODE MODEL

We assess the validity of a minimal form (55) based on the two-mode model. To this end, we consider the GCM in the mean field approximation [6–21], thereby determining not only the minimal form without the knowledge of the inter-replica DCF $\tilde{c}(r)$ (Section VIA) but also the mode numbers, μ and μ' (Section VIB). We compare the present results on the mean overlap Q_{12} of the GCM with the previous ones at high densities where out-of-equilibrium clusters are formed (see Section VIC) [22, 23].

A. Intra-Replica TCF of the GCM in the Liquid State

The two-replica system in the cluster glass phase has been numerically studied for the GCM at higher densities, showing a stepwise increase in the mean overlap Q_{12} : Q_{12} varies infinitesimally within a range of $\tilde{\epsilon}$ and shows a discrete increase at a certain value of $\tilde{\epsilon}$ [22]. Hence, we investigate the GCM in the mean field approximation,

$$\begin{aligned} c(k) &= -v(k) \\ &= -d^3 \tilde{\epsilon} \sqrt{\pi^3} \exp\left(-\frac{k^2}{4}\right), \end{aligned} \quad (60)$$

which has been found to be a good descriptor of the GCM at high densities [1, 2, 6–21]. Equation (60) becomes

$$c(k) = -d^3 \tilde{\epsilon} \sqrt{\pi^3} e^{\frac{b^2 - a^2}{4}} \left\{ \cos\left(\frac{ab}{2}\right) - i \sin\left(\frac{ab}{2}\right) \right\} \quad (61)$$

when considering the complex wavenumber $k = a + ib$ in units of $1/d$ as before.

Combining Equations (30) and (61) in the above mean field approximation, the pole equation in the liquid state is expressed as

$$1 + \phi \tilde{\epsilon} \sqrt{\pi^3} e^{\frac{b^2 - a^2}{4}} \cos\left(\frac{ab}{2}\right) = 0, \quad (62)$$

$$\sin\left(\frac{ab}{2}\right) = 0. \quad (63)$$

Equations (62) and (63) reduce to

$$\phi \tilde{\epsilon} \sqrt{\pi^3} e^{\frac{b^2 - a^2}{4}} = 1, \quad (64)$$

$$\frac{ab}{2} = (2m - 1)\pi, \quad (65)$$

with m denoting the natural number. The m th mode introduced after Equation (40) is traced back to the relation (65).

Let us then consider the 3D Fourier transform of $h_\sigma(k)$ ($\sigma = +, -$) as follows:

$$r h_\sigma(r) = \frac{1}{4i\pi^2 d^3} \int_{-\infty}^{\infty} dk k e^{ikr} h_\sigma(k). \quad (66)$$

We evaluate the RHS of Equation (66) using contour integral along an infinite-radius semicircle in the complex upper half-plane. To perform the contour integral, we need to find the poles of Equations (62) and (63). Considering the four poles, $k_n^\sigma = a_n^\sigma + ib_n^\sigma$ and $k_{-n}^\sigma = -a_n^\sigma + ib_n^\sigma$ with $a_{-n}^\sigma = -a_n^\sigma$ and $b_{-n}^\sigma = b_n^\sigma$, Equation (66) yields

$$r h_\sigma(r) = \frac{1}{2\pi} \sum_{m \geq 1} \sum_{n=m, -m} k_n^\sigma e^{ik_n^\sigma r} \text{Res}[h_\sigma(k_n^\sigma)], \quad (67)$$

where the residue $\text{Res}[h_\sigma(k_n^\sigma)]$ of $h_\sigma(k_n^\sigma)$ at a pole k_n^σ reads

$$\text{Res}[h_\sigma(k_n^\sigma)] = \frac{-c_\sigma(k_n^\sigma)}{2\phi c'_\sigma(k_n^\sigma)}, \quad (68)$$

using $c'_\sigma(k_n^\sigma) = dc_\sigma(k)/dk|_{k=k_n^\sigma}$.

In the mean field approximation of Equation (60), we have $c'_\sigma(k) = -v'(k) = (k/2)v(k)$ for the GCM in the liquid state. Accordingly, it follows from Equations (67) and (68), as well as the requirement [RR], that the liquid-state TCF, $h^{\text{liq}}(r) = h_+(r) + h_-(r)$, in the GCM is given by

$$\begin{aligned} rh^{\text{liq}}(r) &= \frac{1}{\pi} \sum_{m \geq 1} \sum_{n=m, -m} e^{-b_n r} e^{i a_n r} \frac{k_n v(k_n)}{-2\phi v'(k_n)} \\ &= \frac{2}{\pi\phi} \sum_{m \geq 1} e^{-b_m r} \cos(a_m r), \end{aligned} \quad (69)$$

implying that $A_m = 1/(\pi\phi)$ and $\theta_m = 0$ in Equation (42).

B. Two Mode Numbers Selected

For comparison with previous results [22], it is necessary to select the specific mode numbers of μ and μ' based on the underlying physics of [FR] for the GCM in the cluster glass phase. Section V C has demonstrated the relevance of the following two characteristic scales to the hierarchical dynamics in the cluster glass phase [23–28]: one length is the mean cluster diameter ξ_L in Equation (58), whereas the other is the average size ξ_S ($< \xi_L$) of rattler cages in Equation (59).

Equations (64) and (65) allow us to calculate the real part of the first pole (i.e., $k_1 = a_1 + ib_1$). As a result, we have $a_1 \approx 5.6$ at $\phi = 0.45$ and $\tilde{\epsilon}^{-1} \times 10^3 = 1.25$, which is in good agreement with the main peak wavenumber of the intra-replica structure factor obtained numerically at the same condition in the cluster glass phase [22]. Furthermore, the non-ergodic behavior of density fluctuations becomes obvious at the main peak wavenumber, which has also been demonstrated using the non-ergodicity factor of the GCM in glassy states [23]. These previous results on the GCM support the validity of Equation (58) at $\mu = 1$; while $S_-(k)$ equals zero at the first pole $k = k_1$ of $h^{\text{liq}}(k)$, the first mode represented by k_1 serves as a principal contribution to the p - p density correlations, or $h_+(r)$.

Combining the above discussion with the relations (58) and (59), we find

$$\mu = 1, \mu < \mu' \quad (70)$$

as well as $\delta = \delta' = 0$, ensuring $\tilde{h}(0) > 0$ in Equation (56). It is plausible to suppose that the increase in $\tilde{\epsilon}$ (or lowering the normalized temperature) results in the decrease in ξ_S due to the cage-size reduction. Thus, the relation (59) implies that the increment in the mode number μ' occurs with the gradual increase in $\tilde{\epsilon}$.

C. Comparison with Previous Results

Equation (69) allows us to rewrite Equations (55)–(57) as

$$r\tilde{h}(r) = \frac{2}{\pi\phi}(1 + \delta)e^{-b_\mu r} \cos(a_\mu r) - \frac{2}{\pi\phi}(1 + \delta')e^{-b_{\mu'} r} \cos(a_{\mu'} r), \quad (71)$$

$$\tilde{h}(0) = \frac{2}{\pi\phi}(b_{\mu'} - b_\mu) + \frac{2}{\pi\phi}(\delta - \delta') \lim_{r \rightarrow 0} \frac{1}{r}, \quad (72)$$

at $\delta = \delta' = 0$.

In Figure 3, there are four curves of $\tilde{g}(r) = 1 + \tilde{h}(r)$ depicted using Equations (70) and (71). Curve 3 depicts Equation (71) without the second term on the RHS, which corresponds to an approximate profile of $\tilde{h}(r)$ in the limit of $\mu' \rightarrow \infty$. We have finite values of $\tilde{h}(0)$ for curves 1 and 2 at $\delta = \delta' = 0$, as implied by Equation (72); otherwise, $\tilde{h}(r)$ diverges at $r = 0$ (see curves 3 and 4).

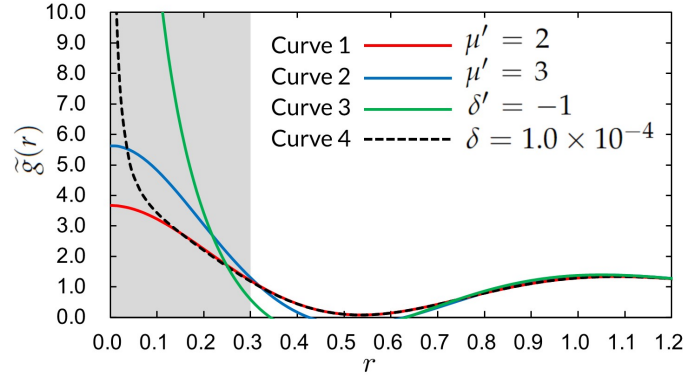


FIG. 3: All curves represent the inter-replica correlation function, $\tilde{g}(r) = 1 + \tilde{h}(r)$, given by Equation (71) in the mean field approximation of the GCM at $\phi = 0.45$. The solid lines show results under the same conditions as those in Table II: the red and blue lines show the profiles at $(\mu', \tilde{\epsilon}^{-1} \times 10^3) = (2, 1.29)$ and $(3, 1.25)$, respectively, and the green line is the result in the absence of the μ' th mode (i.e., $\delta = 0$ and $\delta' = -1$ in Equation (71)) at $\tilde{\epsilon}^{-1} \times 10^3 = 1.17$. The broken line shows a divergent behavior when making a difference such that $\delta = 1.0 \times 10^{-4}$ and $\delta' = 0$ at $(\mu', \tilde{\epsilon}^{-1} \times 10^3) = (2, 1.29)$. The gray area indicates a range where the mean overlap Q_{12} is calculated using Equations (73)–(75).

Figure 3 shows the following:

- $\tilde{h}(0) = \tilde{g}(0) - 1 > 0$ is secured for all curves.
- $\tilde{g}(r) \geq 0$ (or $\tilde{h}(r) \geq -1$) holds for $0 \leq r \leq l$ when adopting $l = 0.3$ in Equation (2), according to the previous results [22].
- We can find a location or region of $0.3 < r < 1$ where either $d\tilde{g}(r)/dr = 0$ or $\tilde{g}(r) = 0$ is satisfied.

These features indicate that there is a depletion region due to the formation of a molecular cluster (or a cluster complex of two replicas) well separated from other clusters.

Figure 3 demonstrates that we can use the expression (71) in Equation (18) because of $\tilde{h}(r) \geq -1$ in the range of $0 \leq r \leq l = 0.3$. Substitution of Equation (71) and $l = 0.3$ into Equation (18) yields

$$Q_{12} - Q_r = 8 \{ (1 + \delta)I(a_1, b_1) - (1 + \delta')I(a_{\mu'}, b_{\mu'}) \}, \quad (73)$$

$$\begin{aligned} I(a, b) &= \int_0^{0.3} dr r e^{-br} \cos(ar) \\ &= J(0.3) - J(0), \end{aligned} \quad (74)$$

where

$$J(x) = \frac{e^{-bx}}{(a^2 + b^2)^2} \{ 2ab \sin(ax) + (a^2 - b^2) \cos(ax) \} + \frac{x e^{-bx}}{a^2 + b^2} \{ a \sin(ax) - b \cos(ax) \}. \quad (75)$$

We see from Equations (72) and (73) that the change from $\delta = 0$ to $\delta = 1 \times 10^{-4}$ at $\delta' = 0$ leads to a negligible increase in Q_{12} , though $\tilde{h}(0)$ diverges due to the slight shift of δ .

In Table II, we assess whether Equations (70) to (75) explain the discrete increases in Q_{12} observed when lowering the normalized temperature in cluster glasses of the GCM. Table II presents the $\tilde{\epsilon}$ -dependencies of Q_{12} at three densities ($\phi = 0.43, 0.45$, and 0.495) obtained from the previous numerical study [22]. We calculate Q_{12} at different mode numbers using Equations (73)–(75), which are compared with the previous results in Table II. We see from Table II that the discrete increase in Q_{12} can be reproduced by the increase in the mode number μ' at different densities using our theory.

It is instructive to compare the profiles of solid lines (curves 1 to 3) in Figure 3 and the mean overlap values given in Table II. On the one hand, Figure 3 indicates that the molecular cluster is more compact and more condensed with the increase in mode number μ' . On the other hand, Table II confirms that Q_{12} always increases by raising μ' consistently with Equations (73)–(75). From combining these results, we find that the variation in Q_{12} is accompanied by a sequential change as follows: the larger the degree of clusters in each replica is by lowering the temperature, the sharper the profile of the inter-replica TCF $\tilde{h}(r)$ is around $r = 0$, thereby showing a discontinuous jump in the mean overlap Q_{12} .

TABLE II: The mean overlap Q_{12} of the GCM at $\phi = 0.43, 0.45$ and 0.495 . There are two kinds of Q_{12} for each density: the upper row represents our theoretical results at the same normalized temperatures as those of previous results, whereas the lower row previous numerical results [22] where the values of $\tilde{\epsilon}^{-1} \times 10^3$ in parentheses correspond to normalized temperatures. The mean values of $\tilde{\epsilon}$ and Q_{12} in each band are adopted as the previous results (see Fig. 3(a) in Ref. [22]). While the theoretical results at mode numbers $\mu' = 2$ to 4 are calculated using eqs. (73) to (75) at $\delta = \delta' = 0$, our results given in the rightmost column ($\delta = 0, \delta' = -1$) are independent of mode numbers and correspond to approximate ones in the limit of $\mu' \rightarrow \infty$ as seen from eq. (73).

ϕ	$\mu' = 2$	$\mu' = 3$	$\mu' = 4$	$\mu' \rightarrow \infty$
0.43	0.10	0.13	0.15	0.17
	0.10 (1.25)	0.12 (1.21)	0.14 (1.17)	–
0.45	0.10	0.13	0.15	0.17
	0.09 (1.29)	0.12 (1.25)	0.15 (1.21)	0.18 (1.17)
0.495	0.10	0.14	0.15	0.18
	0.10 (1.35)	0.16 (1.32)	–	0.20 (1.29)

VII. CONCLUDING REMARKS

Our results consist of three parts. Each part presents the pole-analysis-based expression for the inter-replica TCF $\tilde{h}(r)$, which becomes simple in the later part. (i) The first part (Sections III and IV A) has presented two methods by which to obtain a general form (44) from the pole analysis. (ii) In the second part (Sections IV B and V), we have introduced the two-mode model represented by Equation (55). The second part has further related two characteristic lengths (ξ_L and ξ_S) to the two modes in Equations (58) and (59), respectively, based on insights from the bi-axial FEL (Figure 2) as an illustration of the hierarchical dynamics inherent in cluster glasses. (iii) The last part (Section VI) has applied the two-mode model to the GCM at high densities, thereby leading to the most simplified form (71). Remarkably, Equation (71) yields Equations (73)–(75), the mean overlap Q_{12} obtained in the mean field approximation, which requires no fitting parameters. Table II shows that the analytical expression (73) for Q_{12} gives theoretical results that are in good agreement with those from the previous numerical study [22].

To be clear in our conclusion, we provide additional notes on each part:

- (i) The flow to obtain Equation (44) is summarized in Figure 1, illustrating that two approaches lead to the same form, Equation (44). While the validity of Equation (44) is ensured by two physical requirements ([RR] and [FR]), we can derive Equation (44) from combining the OZ equations (Equations (19) and (20)) and the pole equation (Equation (27)). It is also important to note that spatial isotropy is assumed for TCFs, $h(r)$ and $\tilde{h}(r)$, in the OZ equations. Applying this supposition to cluster glasses is equivalent to assuming the isotropic shape of each cluster. In other words, the morphological diversity of clusters is beyond the scope of this study, taking no account of the surface energy of clusters.
- (ii) Figure 2 illustrates the shift from ON to OFF state associated with switching off the attractive field (i.e., $\tilde{\epsilon}_{12} \rightarrow 0$) when considering the FEL for the two-replica system (i.e., $n = 2$). The applied attractive field allows for two replicas to select the same basin in the y -axis direction of Figure 2b. After switching off the attractive field, two replicas in the cluster glass phase remain trapped in the same basin but are no longer confined within the same sub-basin in the x -axis direction of Figure 2b, which causes the blurring of cage-hopping dynamics.
- (iii) For assessing the analytical theory, we focus on discrete increases in Q_{12} due to lowering the normalized temperature $\tilde{\epsilon}^{-1}$ in cluster glasses of the GCM. We can ascribe the discontinuous change to the second term on the RHS of Equation (71) that arises from the μ' th mode of $h_-(r)$ defined in Equation (22). Surprisingly, Table II supports the validity of our theory by demonstrating that the novel $\tilde{\epsilon}$ -dependencies of Q_{12} can be explained from the mode number μ' that increases by one.

Finally, going back to the general form (44) of the inter-replica TCF, we would like to see what is implied by the difference between the first and second terms on the RHS of Equation (44). On the one hand, the first term with a positive sign in Equation (44) expresses synchronous cluster-scale fluctuations of two replicas confined to the same basin (i.e., fluctuations along the y -axis in Figure 2b). On the other hand, the second term with a negative sign in Equation (44) represents fluctuations along the x -axis in Figure 2b, causing a decrease in inter-replica correlations due

to asynchronous behaviors of different replica particles such as vibration around different sub-basins and transition to other sub-basins.

The theoretical development would help us understand the underlying physics of cluster glasses. First, recall that the GCM discussed in Section VI corresponds to a standard model of polymeric systems [1, 2]. Additionally, colloidal systems with competing interactions (short-range attractive and long-range repulsive interactions) as well as the Q^\pm class in the GEM vitrify while forming equilibrium clusters with diverse morphologies [56, 62]. For any of these systems, the pole-analysis-based discussions are valid. Specifically, the two-mode model, which focuses on two lengths (cluster and particle scales), is suitable for investigating the FELs in cluster glasses as detailed in Section V. Our two-replica theory can also address the dynamical heterogeneity in realistic glassy systems because the overlap correlation function provides the four-point correlation function, a significant measure of dynamic heterogeneity [63, 64]. Therefore, our simple method of evaluating overlap could offer a promising approach to investigate dynamical issues in glassy systems with hierarchical structures, including cluster glasses. However, it remains necessary to compare experimental and simulation results for various glassy systems with our theoretical ones obtained from more accurate forms of the DCFs, which will allow us to gain deeper insights into the cluster glass phase.

Nomenclature

GEM	generalized exponential model
GCM	Gaussian core model
FEL	free-energy landscape
TCF	total correlation function
DCF	direct correlation function
OZ equation	Ornstein–Zernike equation
$v(r)$	interaction potential in units of $k_B T$
r	interparticle distance in units of a characteristic length d
$\tilde{\epsilon}$	dimensionless interaction strength at zero separation
$\hat{\rho}_\alpha(\mathbf{x})$	microscopic density in replica α of N -particle system
$Q_{\alpha\beta}$	mean overlap between configurations of replica α and replica β
$\phi = \bar{\rho}d^3$	volume fraction defined using a uniform density $\bar{\rho}$
$\hat{\rho}_+(\mathbf{r})$	p -density defined in Equation (7)
$\hat{\rho}_-(\mathbf{r})$	n -density defined in Equation (8)
$h_+(r)$	TCF of p - p density fluctuations defined in Equation (10)
$h_-(r)$	TCF of n - n density fluctuations defined in Equation (11)
$h(r)$	intra-replica TCF
$\tilde{h}(r)$	inter-replica TCF
$c(r)$	intra-replica DCF
$\tilde{c}(r)$	inter-replica DCF
$S_+(k)$	structure factor of p - p density fluctuations defined in Equation (37)
$S_-(k)$	structure factor of n - n density fluctuations defined in Equation (37)

-
- [1] Likos, C.N. Effective interactions in soft condensed matter physics. *Phys. Rep.* **2001**, *348*, 267–439.
 - [2] Likos, C.N. Soft matter with soft particles. *Soft Matter* **2006**, *2*, 478–498
 - [3] van Hecke, M. Jamming of soft particles: Geometry, mechanics, scaling and isostaticity. *J. Phys. Condens. Matter* **2009**, *22*, 033101.
 - [4] Cinti, F.; Macrì, T.; Lechner, W.; Pupillo, G.; Pohl, T. Defect-induced supersolidity with soft-core bosons. *Nat. Commun.* **2014**, *5*, 3235.
 - [5] Díaz-Méndez, R.; Mezzacapo, F.; Lechner, W.; Cinti, F.; Babaev, E.; Pupillo, G. Glass transitions in monodisperse cluster-forming ensembles: Vortex matter in type-1.5 superconductors. *Phys. Rev. Lett.* **2017**, *118*, 067001.
 - [6] Ikeda, A.; Miyazaki, K. Glass transition of the monodisperse Gaussian core model. *Phys. Rev. Lett.* **2011**, *106*, 015701.
 - [7] Ikeda, A.; Miyazaki, K. Thermodynamic and structural properties of the high density Gaussian core model. *J. Chem. Phys.* **2011**, *135*, 024901.
 - [8] Ikeda, A.; Miyazaki, K. Slow dynamics of the high density gaussian core model. *J. Chem. Phys.* **2011**, *135*, 054901.
 - [9] Coslovich, D.; Bernabei, M.; Moreno, A.J. Cluster glasses of ultrasoft particles. *J. Chem. Phys.* **2012**, *137*, 184904.
 - [10] Coslovich, D.; Ikeda, A. Cluster and reentrant anomalies of nearly Gaussian core particles. *Soft Matter* **2013**, *9*, 6786–6795.
 - [11] Coslovich, D.; Ikeda, A.; Miyazaki, K. Mean-field dynamic criticality and geometric transition in the Gaussian core model. *Phys. Rev. E* **2016**, *93*, 042602.
 - [12] Miyazaki, R.; Kawasaki, T.; Miyazaki, K. Cluster glass transition of ultrasoft-potential fluids at high density. *Phys. Rev. Lett.* **2016**, *117*, 165701.
 - [13] Miyazaki, R.; Kawasaki, T.; Miyazaki, K. Slow dynamics coupled with cluster formation in ultrasoft-potential glasses. *J. Chem. Phys.* **2019**, *150*, 074503.
 - [14] Louis, A.A.; Bolhuis, P.G.; Hansen, J.P. Mean-field fluid behavior of the Gaussian core model. *Phys. Rev. E* **2000**, *62*, 7961.
 - [15] Lang, A.; Likos, C.N.; Watzlawek, M.; Löwen, H. Fluid and solid phases of the Gaussian core model. *J. Phys. Condens. Matter* **2000**, *12*, 5087.
 - [16] Likos, C.N.; Lang, A.; Watzlawek, M.; Löwen, H. Criterion for determining clustering versus reentrant melting behavior for bounded interaction potentials. *Phys. Rev. E* **2001**, *63*, 031206.
 - [17] Mladek, B.M.; Gottwald, D.; Kahl, G.; Neumann, M.; Likos, C.N. Formation of polymorphic cluster phases for a class of models of purely repulsive soft spheres. *Phys. Rev. Lett.* **2006**, *96*, 045701.
 - [18] Mladek, B.M.; Gottwald, D.; Kahl, G.; Neumann, M.; Likos, C.N. Clustering in the absence of attractions: Density functional theory and computer simulations. *J. Phys. Chem. B* **2007**, *111*, 12799–12808.
 - [19] Likos, C.N.; Mladek, B.M.; Gottwald, D.; Kahl, G. Why do ultrasoft repulsive particles cluster and crystallize? Analytical results from density-functional theory. *J. Chem. Phys.* **2007**, *126*, 224502.
 - [20] Pini, D.; Parola, A.; Reatto, L. An unconstrained DFT approach to microphase formation and application to binary Gaussian mixtures. *J. Chem. Phys.* **2015**, *143*, 034902.
 - [21] Nikiteas, I.; Heyes, D.M. Reentrant melting and multiple occupancy crystals of bounded potentials: Simple theory and direct observation by molecular dynamics simulations. *Phys. Rev. E* **2020**, *102*, 042102.
 - [22] Bomont, J.M.; Likos, C.N.; Hansen, J.P. Glass quantization of the Gaussian core model. *Phys. Rev. E* **2022**, *105*, 024607.
 - [23] Sposini, V.; Likos, C.N.; Camargo, M. Glassy phases of the Gaussian core model. *Soft Matter* **2023**, *19*, 9531–9540.
 - [24] Montes-Saralegui, M.; Nikoubashman, A.; Kahl, G. Merging and hopping processes in systems of ultrasoft, cluster forming particles under compression. *J. Chem. Phys.* **2014**, *141*, 124908.
 - [25] Schwanzler, D.F.; Coslovich, D.; Kahl, G. Two-dimensional systems with competing interactions: Dynamic properties of single particles, and of clusters. *J. Phys. Condens. Matter* **2016**, *28*, 414015.
 - [26] Liu, Y.; Liu, G.; Zhang, W.; Du, C.; Wesdemiotis, C.; Cheng, S.Z. Cooperative soft-cluster glass in giant molecular clusters. *Macromolecules* **2019**, *52*, 4341–4348.
 - [27] Cho, J.H.; Cerbino, R.; Bischofberger, I. Emergence of multiscale dynamics in colloidal gels. *Phys. Rev. Lett.* **2020**, *124*, 088005.
 - [28] Liebetreu, M.; Likos, C.N. Shear-induced stack orientation, and breakup in cluster glasses of ring polymers. *ACS Appl. Polym. Mater.* **2020**, *2*, 3505–3517.
 - [29] Charbonneau, P.; Kurchan, J.; Parisi, G.; Urbani, P.; Zamponi, F. Fractal free energy landscapes in structural glasses. *Nat. Commun.* **2014**, *5*, 3725.
 - [30] Müller, M.; Wyart, M. Marginal stability in structural, spin, and electron glasses. *Annu. Rev. Condens. Matter Phys.* **2015**, *6*, 177–200.
 - [31] Berthier, L.; Biroli, G.; Charbonneau, P.; Corwin, E.I.; Franz, S.; Zamponi, F. Gardner physics in amorphous solids and beyond. *J. Chem. Phys.* **2019**, *151*, 010901.
 - [32] Dennis R.C.; Corwin, E.I. Jamming energy landscape is hierarchical and ultrametric. *Phys. Rev. Lett.* **2020**, *124*, 078002.
 - [33] Hammond, A.P.; Corwin, E.I. Experimental observation of the marginal glass phase in a colloidal glass. *Proc. Natl. Acad. Sci. USA* **2020**, *117*, 5714–5718.
 - [34] Ikeda, H.; Miyazaki, K.; Yoshino, H.; Ikeda, A. Multiple glass transitions and higher-order replica symmetry breaking of binary mixtures. *Phys. Rev. E* **2021**, *103*, 022613.
 - [35] Arceri, F.; Corwin, E.I.; O’Hern, C.S. The jamming transition and the marginally stable solid. In *Spin Glass Theory and Far Beyond: Replica Symmetry Breaking after 40 Years*; Marinari, E., Mézard, M., Parisi, G., Ricci-Tersenghi, F., Sicuro,

- G., Zamponi, F., Eds.; World Scientific: Singapore, 2023; pp. 239–254.
- [36] Franz, S.; Parisi, G. Phase diagram of coupled glassy systems: A mean-field study. *Phys. Rev. Lett.* **1997**, *79*, 2486–2489.
- [37] Franz, S.; Parisi, G. Effective potential in glassy systems: Theory and simulations. *Phys. Rev. E* **1998**, *261*, 317–339.
- [38] Cardenas, M.; Franz, S.; Parisi, G. Constrained Boltzmann–Gibbs measures and effective potential for glasses in hypernetted chain approximation and numerical simulations. *J. Chem. Phys.* **1999**, *110*, 1726–1734.
- [39] Franz, S.; Parisi, G. On non-linear susceptibility in supercooled liquids. *J. Phys. Condens. Matter* **2000**, *12*, 6335.
- [40] Jack, R.L.; Berthier, L. The melting of stable glasses is governed by nucleation-and-growth dynamics. *J. Chem. Phys.* **2016**, *144*, 244506.
- [41] Guiselin, B.; Berthier, L.; Tarjus, G. Statistical mechanics of coupled supercooled liquids in finite dimensions. *SciPost Phys.* **2022**, *12*, 091.
- [42] Frusawa, H. Replica Field Theory for a Generalized Franz–Parisi Potential of Inhomogeneous Glassy Systems: New Closure and the Associated Self-Consistent Equation. *Entropy* **2024**, *26*, 241.
- [43] Berthier, L. Overlap fluctuations in glass-forming liquids. *Phys. Rev. E* **2013**, *88*, 022313.
- [44] Parisi, G.; Seoane, B. Liquid-glass transition in equilibrium. *Phys. Rev. E* **2014**, *89*, 022309.
- [45] Bomont, J.M.; Hansen, J.P.; Pastore, G. An investigation of the liquid to glass transition using integral equations for the pair structure of coupled replica. *J. Chem. Phys.* **2014**, *141*, 174505.
- [46] Bomont, J.M.; Hansen, J.P.; Pastore, G. Hypernetted-chain investigation of the random first-order transition of a Lennard-Jones liquid to an ideal glass. *Phys. Rev. E* **2015**, *92*, 042316.
- [47] Bomont, J.M.; Pastore, G. An alternative scheme to find glass state solutions using integral equation theory for the pair structure. *Mol. Phys.* **2015**, *113*, 2770–2775.
- [48] Bomont, J.M.; Hansen, J.P.; Pastore, G. Revisiting the replica theory of the liquid to ideal glass transition. *J. Chem. Phys.* **2019**, *150*, 154504.
- [49] Bomont, J.M.; Pastore, G.; Hansen, J.P. Coexistence of low and high overlap phases in a supercooled liquid: An integral equation investigation. *J. Chem. Phys.* **2019**, *146*, 114504.
- [50] Evans, R.; Leote de Carvalho, R.J.F.; Henderson, J.R.; Hoyle, D.C. Asymptotic decay of correlations in liquids and their mixtures. *J. Chem. Phys.* **1994**, *100*, 591–603.
- [51] Dijkstra, M.; Evans, R. A simulation study of the decay of the pair correlation function in simple fluids. *J. Chem. Phys.* **2000**, *112*, 1449–1456.
- [52] Grodon, C.; Dijkstra, M.; Evans, R.; Roth, R. Decay of correlation functions in hard-sphere mixtures: Structural crossover. *J. Chem. Phys.* **2004**, *121*, 7869–7882.
- [53] Archer, A.J.; Pini, D.; Evans, R.; Reatto, L. Model colloidal fluid with competing interactions: Bulk and interfacial properties. *J. Chem. Phys.* **2007**, *126*, 014104.
- [54] Walters, M.C.; Subramanian, P.; Archer, A.J.; Evans, R. Structural crossover in a model fluid exhibiting two length scales: Repercussions for quasicrystal formation. *Phys. Rev. E* **2018**, *98*, 012606.
- [55] Cats, P.; Evans, R.; Härtel, A.; van Roij, R. Primitive model electrolytes in the near, and far field: Decay lengths from DFT, and simulations. *J. Chem. Phys.* **2021**, *154*, 124504.
- [56] Kliks, C.L.; Royall, C.P.; Tanaka, H. Structural and dynamical features of multiple metastable glassy states in a colloidal system with competing interactions. *Phys. Rev. Lett.* **2010**, *104*, 165702.
- [57] Tsurusawa, H.; Leocmach, M.; Russo, J.; Tanaka, H. Direct link between mechanical stability in gels and percolation of isostatic particles. *Sci. Adv.* **2019**, *5*, eaav6090.
- [58] Ruiz-Franco, J.; Zaccarelli, E. On the role of competing interactions in charged colloids with short-range attraction. *Annu. Rev. Condens. Matter Phys.* **2021**, *12*, 51–70.
- [59] Tan, J.; Afify, N.D.; Ferreiro-Rangel, C.A.; Fan, X.; Sweatman, M.B. Cluster formation in symmetric binary SALR mixtures. *J. Chem. Phys.* **2021**, *154*, 074504.
- [60] Costa, D.; Munaó, G.; Bomont, J.M.; Malescio, G.; Palatella, A.; Prestipino, S. Microphase versus macrophase separation in the square-well-linear fluid: A theoretical and computational study. *Phys. Rev. E* **2023**, *108*, 034602.
- [61] Patsahan, O.; Meyra, A.; Ciach, A. Spontaneous pattern formation in monolayers of binary mixtures with competing interactions. *Soft Matter* **2024**, *20*, 1410–1424.
- [62] Bomont, J.M.; Pastore, G.; Costa, D.; Munaó, G.; Malescio, G.; Prestipino, S. Arrested states in colloidal fluids with competing interactions: A static replica study. *J. Chem. Phys.* **2024**, *160*, 214504.
- [63] Franz, S.; Jacquin, H.; Parisi, G.; Urbani, P.; Zamponi, F. Static replica approach to critical correlations in glassy systems. *J. Chem. Phys.* **2013**, *138*, 12A540.
- [64] Foleña, G.; Biroli, G.; Charbonneau, P.; Hu, Y.; Zamponi, F. Equilibrium fluctuations in mean-field disordered models. *Phys. Rev. E* **2022**, *106*, 024605.